JACS
JOURNAL OF THE AMERICAN CHEMICAL SOCIETY
pubs.acs.org/JACS
Article

Spontaneously Blinking Fluorophores Based on Nucleophilic Addition/Dissociation of Intracellular Glutathione for Live-Cell Super-resolution Imaging

Akihiko Morozumi, Mako Kamiya,* Shin-nosuke Uno, Keitaro Umezawa, Ryosuke Kojima, Toshitada Yoshihara, Seiji Tobita, and Yasuteru Urano*

Cite This: J. Am. Chem. Soc. 2020, 142, 9625−9633
Read Online

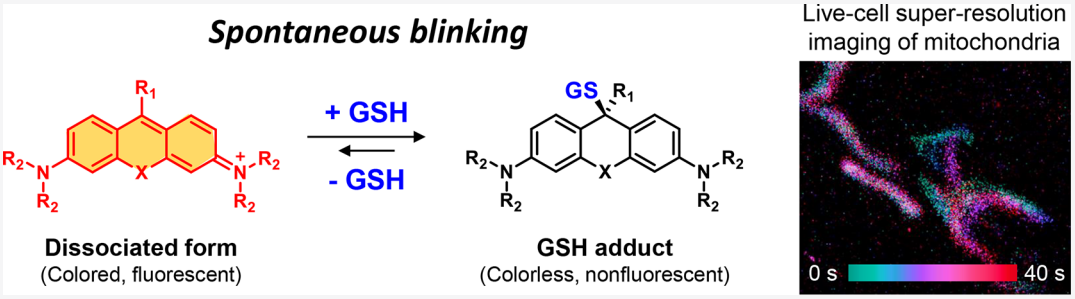

ABSTRACT: Single-molecule localization microscopy (SMLM) allows the reconstruction of super-resolution images but generally requires prior intense laser irradiation and in some cases additives to induce blinking of conventional fluorophores. We previously introduced a spontaneously blinking rhodamine fluorophore based on an intramolecular spirocyclization reaction for live-cell SMLM under physiological conditions. Here, we report a novel principle of spontaneous blinking in living cells, which utilizes reversible ground-state nucleophilic attack of intracellular glutathione (GSH) upon a xanthene fluorophore. Structural optimization afforded two pyronine fluorophores with different colors, both of which exhibit equilibrium (between the fluorescent dissociated form and the nonfluorescent GSH adduct form) and blinking kinetics that enable SMLM of microtubules or mitochondria in living cells. Furthermore, by using spontaneously blinking fluorophores working in the near-infrared (NIR) and green ranges, we succeeded in dual-color live-cell SMLM without the need for optimization of the imaging medium.

INTRODUCTION

Super-resolution fluorescence imaging provides microscopic images with a resolution well below the diffraction limit and is a powerful tool for detailed investigation of cellular structures and processes.[1−5] Single-molecule localization microscopy (SMLM) is one of the most frequently used methods and reconstructs super-resolution images through detection and high-precision localization of individual fluorescent molecules attached to the observation target.[2,6] In order to perform SMLM with conventional organic fluorophores, approaches known as direct stochastic optical reconstruction microscopy (dSTORM)[7] or ground-state depletion microscopy followed by individual molecule return (GSDIM)[8] have been developed. These methods require the fluorophores to be converted into a dark state via the excited state and then to revert stochastically to the fluorescent state under intense laser irradiation in the presence of reducing agents such as thiols.[2,9] However, intense laser irradiation can be cytotoxic and may cause photobleaching of the fluorophores; also, especially in the context of multicolor SMLM, it can be difficult to find a suitable composition of the imaging buffer to induce appropriate blinking states of multiple fluorophores.[2,10,11]

We previously reported a first-in-class spontaneously blinking fluorophore, HMSiR, based on an intramolecular spirocyclization reaction in the ground state. This fluorophore exists mostly in a colorless and nonfluorescent form and spontaneously blinks with fluorescence emission in the near-infrared (NIR) range. In contrast to conventional fluorophores, HMSiR does not require intense laser irradiation or any additive for blinking, so it is suitable for live-cell SMLM under physiological conditions.[12] In order to expand the color range of spontaneously blinking fluorophores, we also developed a spontaneously blinking fluorophore with green-light emission, HEtetTFER, and by using the two fluorophores, we succeeded in dual-color SMLM

Received: January 13, 2020
Published: April 28, 2020

of fixed cells in additive-free buffer solution without optimization.[10] Unfortunately, however, we found that HEtetTFER could not be used for live-cell SMLM, probably due to an unfavorable subcellular localization, poor cell-membrane permeability, or other reasons. These results clearly demonstrate that spontaneously blinking fluorophores that work in vitro do not always work in live cells, and therefore we need to prepare a variety of candidate blinking fluorophores and select those that can work in live cells in order to achieve dual-color live-cell SMLM.

Here, in order to expand the molecular design strategy of spontaneously blinking fluorophores, we develop a novel principle of spontaneous blinking in living cells, which builds on our previous finding that some xanthene fluorophores convert between a colored, fluorescent form and a colorless, nonfluorescent form as a result of a reversible ground-state nucleophilic attack of intracellular glutathione (GSH) upon the 9th carbon atom of the xanthene ring (Figure 1). We previously utilized this thermal equilibrium of intermolecular nucleophilic addition/dissociation to develop a reversible fluorescent probe for monitoring intracellular GSH concentration. The probe has a suitable dissociation constant toward GSH ($K_{d,GSH}$) of millimolar level and a subsecond response rate for real-time monitoring of intracellular GSH dynamics.[13] In particular, we thought that the lack of background fluorescence of the GSH adduct in this thermal equilibrium would be advantageous for achieving high localization precision in SMLM. In order to utilize this intermolecular reaction for SMLM, it is essential to ensure that only a small subset of the fluorophores is switched on, followed by stochastic reversion to the nonfluorescent state with appropriate kinetics.[12] Therefore, we started by derivatizing xanthene fluorophores to look for candidate fluorophores with appropriate $K_{d,GSH}$ values and blinking kinetics. As a result, we found two candidate fluorophores, SiP650 and CP550, working in the NIR and green wavelength ranges, respectively, with which we were able to perform SMLM of microtubules in living cells by utilizing the endogenous intracellular GSH. Furthermore, we achieved dual-color live-cell SMLM by using CP550 together with our previously developed NIR spontaneously blinking fluorophore, HMSiR, and succeeded in observing two targets in mammalian cells and in bacterial cells without the need for optimization of the imaging medium.

RESULTS AND DISCUSSION

Design and Synthesis of Novel Blinking Fluorophores: Evaluation of Thermal Equilibrium of Addition and Dissociation of GSH. In order to develop a new class of spontaneously blinking fluorophores for SMLM based on intermolecular nucleophilic addition/dissociation of intracellular GSH (Figure 1a), we considered that it would be essential to optimize two parameters: (1) the dissociation constant toward GSH ($K_{d,GSH}$), so that a small subset of fluorophores would exist in the fluorescent state in the physiological GSH concentration range, in order to avoid overlapping signals; (2) the lifetime of the fluorescent form (τ, the duration until the fluorescent dissociated form reverts to the nonfluorescent GSH adduct form) in order to match the exposure time of microscope cameras so that sufficient photons can be detected for precise localization.[12]

We first tried to optimize the $K_{d,GSH}$ values of xanthene derivatives to control the percentage of the fluorescent dissociated form at physiological GSH concentrations of 1−10 mM.[14,15] The $K_{d,GSH}$ value can be determined from the dose−response curve of the fluorophore as the GSH concentration at which the absorbance of the dissociated form is reduced to half of the maximum (Figure 1c). When the $K_{d,GSH}$ value of a fluorophore is 1 mM, as is the case with silicon-substituted rhodamine 2′Me SiR600 (Figure 1b),[13] more than 10% of the fluorophore exists in the fluorescent dissociated form in the presence of 1−10 mM GSH. In contrast, a $K_{d,GSH}$ value of less than 10 μM implies that less than 1% of the fluorophore would

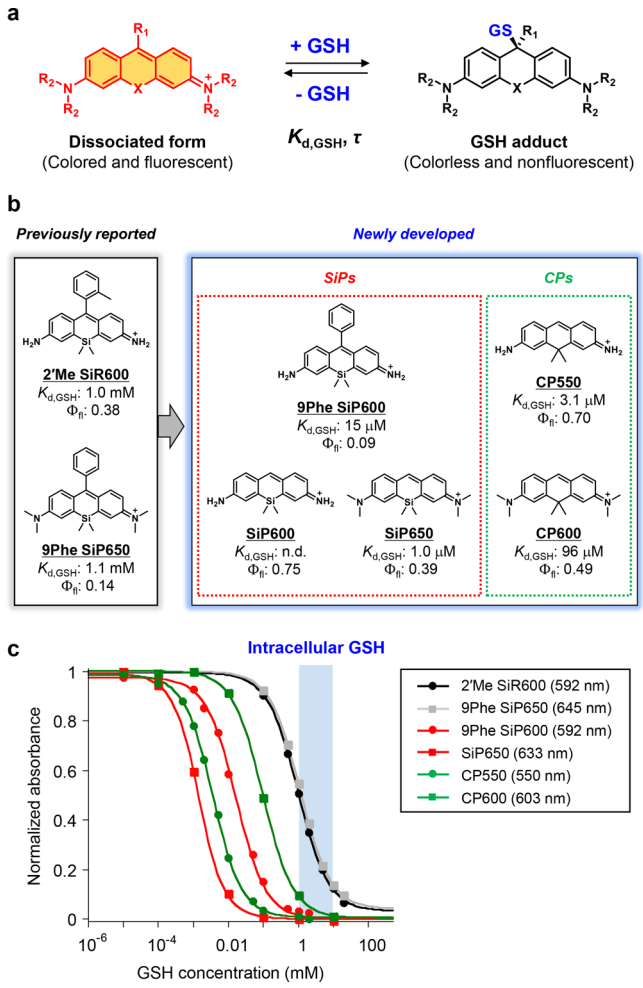

Figure 1. Spontaneously blinking fluorophores for SMLM based on the ground state nucleophilic addition and dissociation of intracellular GSH. (a) Fluorescence switching based on intermolecular nucleophilic addition and dissociation of GSH to and from xanthene derivatives as a novel mechanism of fluorescence blinking for SMLM. Xanthene derivatives can convert between the fluorescent dissociated form and the nonfluorescent GSH adduct form. $K_{d,GSH}$ is the dissociation constant toward GSH, and τ is the lifetime of the dissociated form. (b) Preparation of new xanthene derivatives with sufficiently low $K_{d,GSH}$ values. Chemical structures of candidate fluorophores based on silicon pyronine (SiP) and carbopyronine (CP) scaffolds are shown with the measured $K_{d,GSH}$ values and fluorescence quantum yields (Φ_{fl}). (c) Dose−response curves of the candidate fluorophores versus GSH. The normalized absorbance at the indicated wavelengths (absorption maxima of the dissociated forms) is plotted against GSH concentration to evaluate $K_{d,GSH}$ for each fluorophore. Absorption spectra were measured in 200 mM sodium phosphate buffer (pH 7.4) containing various concentrations of GSH and 1% dimethyl sulfoxide (DMSO) as a cosolvent and normalized with respect to those in the absence of GSH. The $K_{d,GSH}$ of SiP600 was not determined because the majority of the molecules underwent nucleophilic addition of hydroxide ion in 200 mM sodium phosphate buffer (pH 7.4) in the absence of GSH.

https://dx.doi.org/10.1021/jacs.0c00451
J. Am. Chem. Soc. 2020, 142, 9625−9633

be in the fluorescent form and most of it would be in the nonfluorescent GSH adduct form at physiological GSH concentrations. Considering recent advances in multi-emitter localization algorithms,[16−21] we set a criterion for $K_{d,GSH}$ value of roughly 1−100 μM so that the percentage of the fluorescent form would be less than 10%. Since it has been suggested that the affinity of a xanthene fluorophore for GSH or other nucleophiles is correlated with the lowest unoccupied molecular orbital (LUMO) level of the fluorophore and the steric hindrance around the 9th carbon atom of the xanthene ring,[12,13,22] we focused on modifying 2′Me SiR600 and 9Phe SiP650, both of which showed low $K_{d,GSH}$ values in our previous study (1.0 mM and 1.1 mM, respectively),[13] aiming to prepare silicon-substituted xanthene fluorophores with decreased $K_{d,GSH}$ values by reducing the steric hindrance around the 9th carbon atom (Figure 1b). We prepared 9Phe SiP600, SiP600, and SiP650 by removing the methyl group from the pendant phenyl group of 2′Me SiR600 or removing the pendant phenyl group itself from 2′Me SiR600 and 9Phe SiP650. 9Phe SiP600 and SiP650 exhibited $K_{d,GSH}$ values of 15 μM and 1.0 μM, respectively; however, it was difficult to determine the $K_{d,GSH}$ value of SiP600, since nucleophilic attack of hydroxide ion in the buffer solution readily occurred due to the high electrophilicity of the fluorophore (Figures 1c and S1 and Table S1). Further, in order to expand the color range, we also prepared carbopyronine derivatives CP550 and CP600 by replacing the silicon atom at the 10th position of SiP600 and SiP650 with a carbon atom. CP550 and CP600 exhibited increased $K_{d,GSH}$ values of 3.1 μM and 96 μM, respectively, probably due to the increased LUMO energy levels of the fluorophores (Figures 1c and S1 and Table S1). These results strongly suggested that the LUMO energy level of the core xanthene ring and the steric hindrance around the 9th carbon of a xanthene fluorophore are indeed important determinants of the $K_{d,GSH}$ value. Through this derivatization, we obtained four candidates with acceptable $K_{d,GSH}$ values in the range of 1−100 μM (9Phe SiP600, SiP650, CP550, CP600). Among these derivatives, SiP650, CP550, and CP600 showed sufficiently high quantum yields (Φ_{fl} = 0.39, 0.70, and 0.49, respectively), while 9Phe SiP600 exhibited a low fluorescence quantum yield (Φ_{fl} = 0.09), probably due to the rotation of its pendant phenyl ring.[13,23] Low fluorescence quantum yield would be disadvantageous considering that the localization precision of a single molecule essentially depends on the number of photons emitted from the molecule,[24,25] so we excluded 9Phe SiP600 as a candidate. Among the remaining three candidates, we selected two pyronines, SiP650 and CP550, as different-colored candidate scaffolds, since these fluorophores can be efficiently excited by commonly used laser lines. In addition, ^{1}H NMR analyses provided evidence of nucleophilic attack by thiol at the 9th carbon of the xanthene units of SiP650 and CP550 (Figure S2).

Evaluation of Duration of the Dissociated Form by Laser Photolysis. The lifetime of the fluorescent dissociated form (τ) is another critical parameter for spontaneously blinking fluorophores (note, this parameter is not the fluorescence lifetime). We supposed that an appropriate τ value would be one that matches the exposure time of the camera in order to achieve detection of sufficient photons for precise localization,[12] and we set a criterion for τ value of millisecond order, taking account of the exposure time of cameras recently used for SMLM.[2,26]

The τ values of the candidate fluorophores, SiP650 and CP550, were determined by laser photolysis as the time constant of conversion from the fluorescent dissociated form to the nonfluorescent GSH adduct form (Figure S3). In sodium phosphate buffer (pH 7.4) containing physiological concentrations of GSH (1−10 mM), most of the fluorophores exist in colorless, nonfluorescent GSH adduct form. Upon pulsed irradiation with an ultraviolet laser (308 nm), transient absorption decay was observed at a wavelength characteristic of each xanthene fluorophore (Figure S4). As the shape of the transient absorption spectrum corresponded well to that of the dissociated form of the fluorophore (Figure S4), the observed transient absorption and its decay were attributed to the transient dissociation of GSH from the xanthene fluorophore, followed by the readdition of GSH. By fitting the obtained decay curve to a pseudo-first-order equation, we could calculate the τ values of the candidate fluorophores. Although the τ values varied depending on GSH concentration, SiP650 and CP550 exhibited appropriate τ values in the millisecond range in the presence of 1−10 mM GSH (Tables 1 and S2). In the case of 9Phe SiP600, which we excluded from our candidates due to its low fluorescence quantum yield, we observed relatively long τ values, particularly at lower concentrations of GSH, which was probably due to the steric hindrance around the 9th carbon. These results confirm that SiP650 and CP550 are promising candidates as different-colored scaffolds.

Table 1. Properties of SiP650 and CP550 Derivatives[a]

	absorbance maximum (nm)	emission maximum (nm)	fluorescence quantum yield[b]	$K_{d,GSH}$ (μM)	τ[c] (ms) 5 mM GSH
SiP650	633	654	0.39	1.0	1.0
SiP650-BA	636	656	0.46	2.9	2.3
SiP650-HaloTag	639	663	0.52	25	9.9
CP550	550	570	0.70	3.1	0.46
CP550-BA	567	586	0.69	35	1.7
CP550-HaloTag	576	593	0.65	210	7.6

[a]Measured in 200 mM sodium phosphate buffer (pH 7.4), except for τ values measured in 10 mM sodium phosphate buffer (pH 7.4). [b]Absolute quantum yield. [c]Lifetime of the fluorescent dissociated form. Note, this parameter is not the fluorescence lifetime.

Evaluation of the Fluorescence Properties of SiP650 and CP550 by Single-Molecule Fluorescence Imaging. We next examined the fluorescence properties of SiP650 and CP550 by means of single-molecule imaging using total internal reflection fluorescence (TIRF) microscopy. We introduced a ligand unit of HaloTag,[27] one of the most widely used protein tags, into SiP650 and CP550 to prepare SiP650-Halo and CP550-Halo, which were then coupled with a purified HaloTag protein to afford SiP650-HaloTag and CP550-HaloTag as fluorophore−protein conjugates (Figure 2a). These protein conjugates showed larger $K_{d,GSH}$ and τ values than those of their parental small molecules SiP650 and CP550 (Table 1 and Figures S5 and S6), probably because of the increased electron density of the xanthene ring due to the *N*-alkylation or *N*-alkyl extension and the increased steric hindrance around the 9th carbon of the xanthene ring due to the protein labeling. Nevertheless, both the τ values and the $K_{d,GSH}$ values remained almost within the original target range (τ = 9.9 ms for SiP650-HaloTag and 7.6 ms for CP550-HaloTag in the presence of 5 mM GSH; $K_{d,GSH}$ = 25 μM for SiP650-HaloTag and 210 μM for CP550-HaloTag). The percentage of the fluorescent form in the

https://dx.doi.org/10.1021/jacs.0c00451
J. Am. Chem. Soc. 2020, 142, 9625−9633

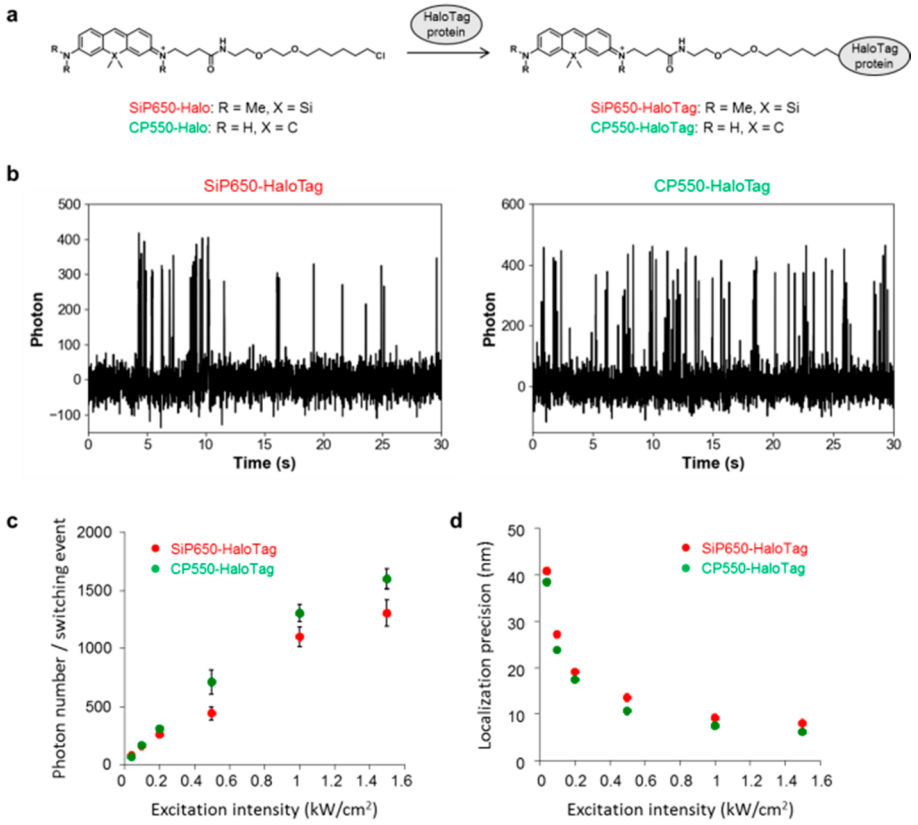

Figure 2. Evaluation of switching properties of the HaloTag protein−fluorophore conjugates by single-molecule fluorescence imaging. (a) Chemical structures of SiP650- and CP550-based HaloTag ligands, and labeling of purified HaloTag proteins to prepare fluorophore−protein conjugates (SiP650-HaloTag, CP550-HaloTag). (b) Single-molecule fluorescence time traces of SiP650-HaloTag (left) and CP550-HaloTag (right). (c, d) Excitation intensity dependence of photon number per switching event (c) and lateral localization precision (d) of SiP650-HaloTag (red) and CP550-HaloTag (green) (mean ± SE, N = 416−12802). Single-molecule imaging was performed in 10 mM sodium phosphate buffer (pH 7.4) containing 5 mM GSH. Excitation 647 nm (100 W/cm^2 for panel b) for SiP650 and 561 nm (100 W/cm^2 for panel b) for CP550. Exposure 8.8 ms/frame.

presence of 5 mM GSH was estimated to be 0.5% for SiP650-HaloTag and 4% for CP550-HaloTag, which would still be within the acceptable range when using multi-emitter localization algorithms.[16−21] However, the $K_{d,GSH}$ values of these conjugates increased further under more acidic pH conditions (Figure S7), indicating that our fluorophores would be less suitable for SMLM at lower pH. We further confirmed that SiP650-HaloTag and CP550-HaloTag exhibit sufficient fluorescence quantum yields (Φ_{fl} = 0.52 and 0.65, respectively) (Table 1), which are comparable to those of the parental small molecules, SiP650 and CP550.

In order to examine the fluorescence properties of SiP650-HaloTag and CP550-HaloTag at the single-molecule level, these fluorophore−protein conjugates were adsorbed onto a coverslip, and their single-molecule fluorescence behaviors were observed with a TIRF microscope in sodium phosphate buffer (pH 7.4) containing 1−10 mM GSH. We confirmed that the majority of SiP650 and CP550 fluorophores existed in the nonfluorescent GSH adduct form, and showed reversible fluorescence blinking even under low-intensity excitation (Figure 2b and Movie S1). The average durations of the fluorescent states of SiP650-HaloTag and CP550-HaloTag were calculated to be 7.4−10 ms and 6.5−12 ms, respectively, in the presence of 1−10 mM GSH, showing clear GSH concentration dependence (Figures S8 and S9). As well as being consistent with the results of the bulk transient absorption measurements, these values meet the criterion for use in SMLM. The number of emitted photons detected per switching event and the localization precision of single molecules varied depending on the laser intensity (40 W/cm^2-1.5 kW/cm^2), and with the highest intensity, we obtained the best values: 1300 photons and 8.0 nm precision for SiP650-HaloTag (647 nm excitation) and 1600 photons and 6.1 nm precision for CP550-HaloTag (561 nm excitation) (Figures 2c,d, S10, and S11). These values are comparable to those of conventional fluorophores used for SMLM (Alexa647[7,28−30] and TMR[28−31]) at the highest laser intensity (1.5 kW/cm^2) in an optimized buffer solution containing β-mercaptoethylamine (MEA) and an enzymatic oxygen scavenging system (GLOX): 1100 photons and 7.3 nm precision for Alexa647-HaloTag conjugate (647 nm excitation) and 300 photons and 15 nm precision for TMR-HaloTag conjugate (561 nm excitation) (Figure S12). These results demonstrated that SiP650-HaloTag and CP550-HaloTag, working in different color regions, both exhibit appropriate blinking for SMLM at physiological GSH concentrations.

Interfering Effects of Other Intracellular Nucleophiles. In order to examine the effects of other intracellular nucleophiles on the optical properties of SiP650 and CP550, we measured the in vitro absorption spectra of SiP650-HaloTag and CP550-HaloTag in the presence of thiol-containing species other than GSH, such as cysteine, homocysteine, and H_2S, at the maximum concentrations possible in a live-cell environment[32−36] (Figures S13 and S14). These thiol-containing species also induced considerable decreases in the absorbance, suggesting that these nucleophiles are reactive with the fluorophores in vitro. Interestingly, the intermolecular reactions with cysteine and

https://dx.doi.org/10.1021/jacs.0c00451
J. Am. Chem. Soc. 2020, 142, 9625−9633

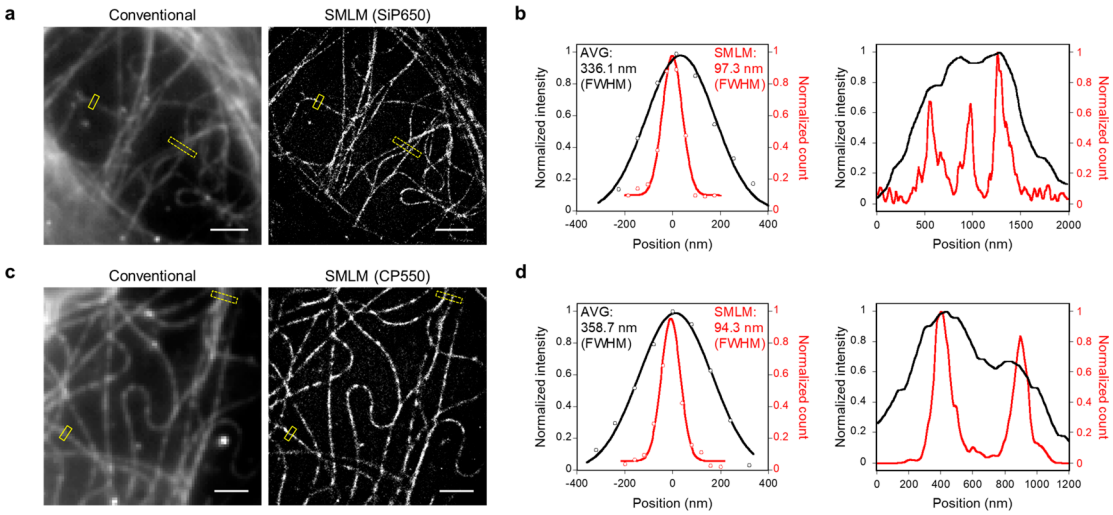

Figure 3. Live-cell SMLM with SiP650-Halo and CP550-Halo. β-Tubulin−Halo fusion proteins were transiently expressed in Vero cells and labeled with SiP650-Halo (a) or CP550-Halo (c) for 30 min. Imaging was performed in cell culture medium (DMEM) after washing. (a, c) Conventional images (averaged projection images, left) and SMLM images (right). Excitation 647 nm (200 W/cm^2) for panel a and 561 nm (200 W/cm^2) for panel c. Acquisition 8.8 ms/frame, 2000 frames (17.6 s) for panel a and 1000 frames (8.8 s) for panel c. (b, d) Transverse profiles of fluorescence intensity in the conventional images (black) and localizations in the SMLM images (red) corresponding to the regions outlined by the solid yellow lines (left) and by the dotted yellow lines (right). Panels b and d correspond to panels a and c, respectively; fwhm = 347.4 ± 25.5 nm (conventional) and 109.2 ± 8.4 nm (SMLM) (mean ± SE, N = 6) for panel b and 339.3 ± 11.1 nm (conventional) and 100.4 ± 5.1 nm (SMLM) (mean ± SE, N = 6) for panel d. Scale bars 3 μm (a) and 2 μm (c).

homocysteine were reversible, whereas the reaction with H_2S was irreversible for some reason (Figure S15). Considering that the physiological concentration of H_2S in living cells is in the sub-micromolar range,[37] this irreversibility should not be an impediment to practical use for live-cell imaging (we were able to obtain images without difficulty) but should be taken into account when the probes are applied to cells with high levels of intracellular H_2S. Further, considering the fact that GSH exists at a much higher concentration than the other nucleophiles in cells, the fluorescence behavior of the fluorophores should be predominantly determined by GSH in live-cell environments. We also confirmed that a physiological concentration of taurine (a representative amine-containing molecule) or a basic pH of 9.0 had little effect on the performance of the fluorophores.

Validation of SiP650 and CP550 for Live-Cell SMLM. Encouraged by the above results, we next attempted to apply our spontaneously blinking fluorophores to live-cell SMLM. First, in order to examine whether the fluorophores could be used to label specific target proteins in living cells, we applied the HaloTag ligands SiP650-Halo and CP550-Halo to Vero cells expressing β-tubulin fused with HaloTag (Figure S16a). SiP650-Halo and CP550-Halo specifically labeled microtubules, indicating that both ligands are cell-permeable and react specifically with the HaloTag proteins (Figure S17a,b). Most importantly, these fluorophores exhibited spontaneous blinking based on the reversible reaction with the endogenous GSH inside the living cells without prior intense laser irradiation and in the absence of any chemical additive (Movies S2 and S3).

We next examined whether SMLM images can be reconstructed from the blinking fluorescence signals of our fluorophores. Because intense laser illumination is not required to induce blinking with our fluorophores, the illumination power can be reduced to minimize photobleaching and potential photodamage. Thousands of consecutive images were recorded at a laser intensity of 200 W/cm^2, which is lower than the illumination power typically required for dSTORM[7,30] or GSDIM,[8] and analyzed to reconstruct a super-resolution image (see Supporting Information for localization analysis employing a multi-emitter fitting algorithm). As a result, the microtubules were visualized more sharply and with better separation than a conventional image (Figure 3), while no obvious cellular structures were constructed when these fluorophores were applied to cells not expressing tag protein (Figure S18a,b). These results indicate that our spontaneously blinking fluorophores enable SMLM with minimal phototoxicity.

Time-Lapse SMLM in Live Cells. In order to expand the utility of our newly developed spontaneously blinking fluorophores, we further prepared SiP650-BnClPy and CP550-BnClPy by introducing a benzylchloropyrimidine (BnClPy) unit, a known substrate for SNAP-tag,[38−40] into SiP650 and CP550, respectively. When we applied these substrates to live Vero cells expressing SNAP-tag proteins in their mitochondria (Figure S16b), we observed efficient labeling of the mitochondria with CP550-BnClPy (Figure S17d), but only subtle labeling was observed with SiP650-BnClPy, probably due to its poor cellular permeability (data not shown). Therefore, we focused on investigating whether super-resolution imaging of mitochondria in living cells can be performed with CP550-BnClPy. Considering the mobility (movement, fusion, or fission) of mitochondria on the time scale of seconds to minutes,[41,42] we recorded thousands of consecutive images at an exposure time of 8.8 ms/frame to match the blinking kinetics of CP550 and then reconstructed sequential SMLM images from partial (500-frame) subsets with 400-frame overlaps (frames 1−500, 101−600, 201−700, 301−800, and so on)[12,43,44] (Figure 4a,b and Movie S4). The resultant SMLM image sequence successfully visualized the dynamics of the mitochondria at a temporal resolution of a few seconds per reconstructed image. We also confirmed that no obvious cellular structures were constructed when CP550-BnClPy was applied to cells not expressing tag protein (Figure S18c). These results suggest that its

https://dx.doi.org/10.1021/jacs.0c00451
J. Am. Chem. Soc. 2020, 142, 9625−9633

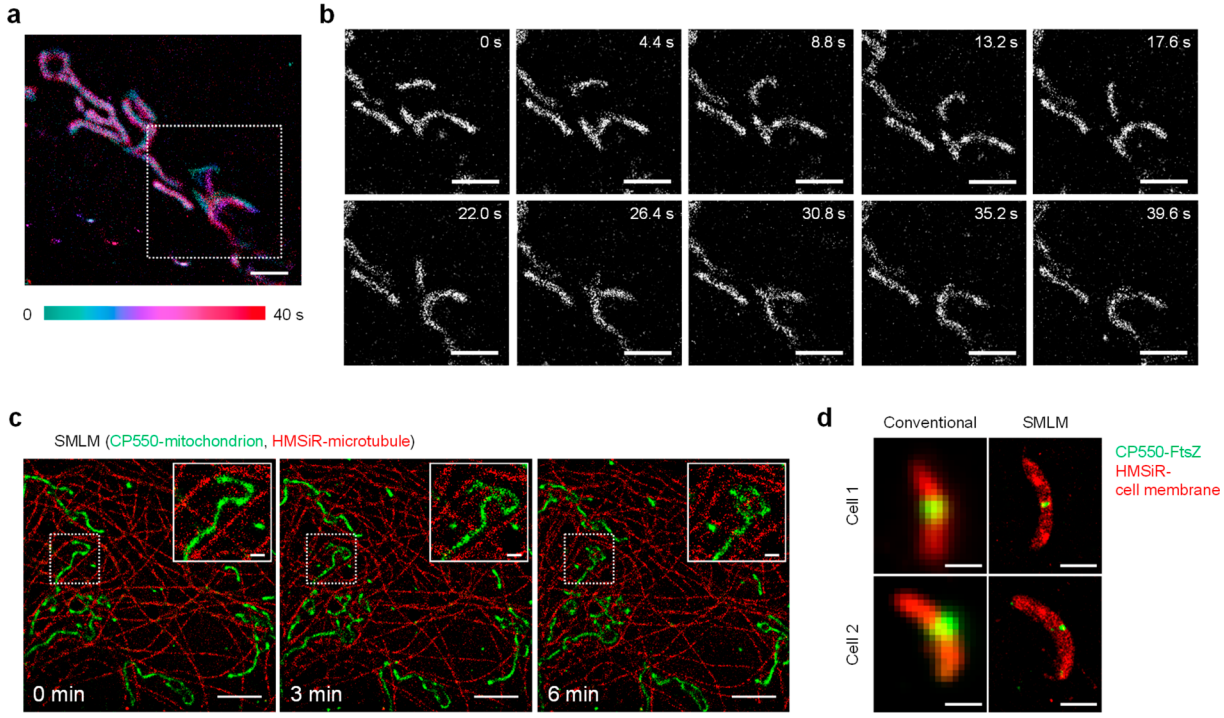

Figure 4. Time-lapse, dual-color live-cell SMLM. (a, b) Time-lapse live-cell SMLM of mitochondria with CP550-BnClPy. Mitochondria-localizable SNAP-tag protein molecules were transiently expressed in living Vero cells and labeled with CP550-BnClPy for 60 min. Imaging was performed in cell culture medium (DMEM). Excitation 561 nm (400 W/cm^2). Acquisition 8.8 ms/frame, 5000 frames (44 s) in total. (a) Subdiffraction localizations collected from the whole data set of 5000 frames. Each localization is color-coded according to the time at which it was detected. (b) Fast time-lapse SMLM image sequence of the region boxed in panel a. Each SMLM image was reconstructed from 500 consecutive frames (4.4 s) starting at the indicated time point. Scale bars 2 μm. (c, d) Dual-color live-cell SMLM with CP550 and HMSiR. (c) Mitochondria-localizable SNAP-tag (green) and β-tubulin−Halo (microtubules, red) were transiently expressed in living Vero cells and labeled with CP550-BnClPy and HMSiR-Halo, respectively, for 60 min. Time-lapse imaging was performed at 0, 3, and 6 min in cell culture medium (DMEM). Significant changes in the mitochondrial structure and arrangement can be seen in the boxed region (dotted boxes), with the magnified views shown in the insets. Laser illumination (561 nm, 300 W/cm^2 for CP550 and 647 nm, 150 W/cm^2 for HMSiR) and image acquisition were performed at 8.8 ms/frame in an alternate manner for the two colors with an 8-frame duration for each turn. Each SMLM image was reconstructed from 960 frames for each color (16.9 s in total). Scale bars 3 μm (main images) and 500 nm (insets). (d) Halo-tagged FtsZ (cell-division-related protein, green) and outer membrane (red) were labeled with CP550-Halo and HMSiR-NHS, respectively, in living *C. crescentus* cells. Imaging was performed on 1.5% agar. Laser illumination (561 nm, 200 W/cm^2 for CP550 and 647 nm, 200 W/cm^2 for HMSiR) and image acquisition were performed at 15 ms/frame in an alternate manner for the two colors with a 7-frame duration for each turn. Each SMLM image (right for each cell) was reconstructed from 7000 frames for each color (210 s in total). Conventional images (averaged projection images, left) were generated from the corresponding raw images. Scale bars 1 μm.

appropriately fast spontaneous blinking rate makes CP550 an excellent choice for tracking mobile targets with minimal damage, perturbation, or artifacts.

Dual-Color SMLM in Live Cells. Multicolor super-resolution imaging has been a powerful tool for detailed studies of biological processes involving multiple cellular components. However, when conventional organic fluorophores are used for multicolor SMLM, it is particularly troublesome to optimize the experimental conditions for inducing appropriate blinking of multiple fluorophores.[2,10,11] Spontaneously blinking fluorophores with different colors would circumvent this difficulty, since their blinking occurs spontaneously under intracellular conditions, without the need for optimization of the imaging buffer composition.[10] Therefore, we next focused on performing dual-color SMLM by utilizing our spontaneously blinking fluorophores with different colors. Specifically, we labeled mitochondria-localized SNAP-tag with CP550-BnClPy and β-tubulin-HaloTag with HMSiR-Halo, a HaloTag ligand of HMSiR, which is our previously reported NIR-emitting, spontaneously blinking fluorophore based on intramolecular spirocyclization (Figure S17c).[12] Irradiation with 561 and 647 nm lasers was applied alternately to excite CP550 and HMSiR, which allowed us to obtain dual-color SMLM images of the mitochondria and the microtubules, respectively, and thus to visualize the relative arrangement of the two targets. Further, as we used a low power level to minimize photobleaching and photodamage, we were able to repeat dual-color SMLM imaging, for example, at 3 min intervals to allow time-lapse experiments (Figure 4c).

Next, we examined whether dual-color SMLM imaging with our spontaneously blinking fluorophores would be applicable to live bacterial cells, which contain structures too tiny to be analyzed by conventional fluorescence microscopy. HaloTag fusion protein of FtsZ,[45] a bacterial cytoskeletal protein forming a part of the cell division machinery (Figure S16c),[46−49] in live *Caulobacter crescentus* bacterial cells was labeled with CP550-Halo, and the outer membrane of the cells was labeled with HMSiR-NHS, an *N*-hydroxysuccinimidyl ester of HMSiR.[12] Then, the bacterial cells were immobilized on an agarose pad for imaging. CP550 showed appropriate blinking inside the bacterial cells, as expected, since the concentration of GSH in bacteria is reported to be in the millimolar range.[50−54] HMSiR also showed spontaneous blinking even on the cell surface, since it blinks on the basis of intramolecular spirocyclization.

https://dx.doi.org/10.1021/jacs.0c00451
J. Am. Chem. Soc. 2020, 142, 9625−9633

Reconstruction of dual-color SMLM images enabled detailed observations of the localizations and structures of protein complexes formed by FtsZ, together with fine profiling of the bacterial morphology by imaging the cell membrane. As previously reported,[46] FtsZ exhibits a continuous band-like pattern (Figure 4d, cell 1) or a spot-like pattern (Figure 4d, cell 2), which cannot be distinguished by conventional microscopy. Further investigations, for example, by three-dimensional[46,55] or time-lapse SMLM,[46] should lead to a better understanding of the distribution and behavior of FtsZ.

CONCLUSION

We have established a novel principle of spontaneous blinking for live-cell SMLM on the basis of nucleophilic addition and dissociation of endogenous intracellular GSH to and from xanthene fluorophores. By structural optimization of the fluorophore, we have developed novel spontaneously blinking fluorophores, SiP650 and CP550, with appropriate equilibrium constants between the fluorescent dissociated form and the nonfluorescent GSH adduct form and with adequately fast blinking kinetics. We confirmed that HaloTag ligands of SiP650 and CP550 can specifically label target proteins and show spontaneous blinking in live cells as a result of reversible nucleophilic attack of intracellular GSH, enabling SMLM images to be obtained. Further, by using CP550 in combination with our NIR-emitting HMSiR, we achieved dual-color live-cell SMLM in mammalian cells and in bacterial cells. Our dual-color approach should be useful for investigating the relationships between two biological targets in live cells with minimal photodamage and without the need to optimize the imaging buffer. We anticipate that the molecular design strategy described in this work can be further applied to develop new fluorophores with different optical properties and blinking kinetics, thereby offering a wider range of tools for super-resolution studies.

ASSOCIATED CONTENT

Supporting Information

The Supporting Information is available free of charge at https://pubs.acs.org/doi/10.1021/jacs.0c00451.

Synthesis and characterization of compounds, evaluation of optical properties and response to GSH, fluorescence imaging, and experimental details (PDF)

Single-molecule fluorescence imaging of fluorophores bound to purified HaloTag proteins (AVI)

Fluorescence blinking of SiP650 bound to β-tubulin-Halo in live cells (AVI)

Fluorescence blinking of CP550 bound to β-tubulin-Halo in live cells (AVI)

Fast time-lapse SMLM of mitochondria in live cells with CP550 (AVI)

AUTHOR INFORMATION

Corresponding Authors

Mako Kamiya − *Graduate School of Medicine, The University of Tokyo, Tokyo 113-0033, Japan; PRESTO, Japan Science and Technology Agency, Kawaguchi, Saitama 332-0012, Japan;* orcid.org/0000-0002-5592-1849; Email: mkamiya@m.u-tokyo.ac.jp

Yasuteru Urano − *Graduate School of Pharmaceutical Sciences and Graduate School of Medicine, The University of Tokyo, Tokyo 113-0033, Japan; AMED-CREST, Japan Agency for Medical Research and Development, Tokyo 100-0004, Japan;* orcid.org/0000-0002-1220-6327; Email: uranokun@m.u-tokyo.ac.jp

Authors

Akihiko Morozumi − *Graduate School of Pharmaceutical Sciences, The University of Tokyo, Tokyo 113-0033, Japan*

Shin-nosuke Uno − *Graduate School of Pharmaceutical Sciences, The University of Tokyo, Tokyo 113-0033, Japan*

Keitaro Umezawa − *Graduate School of Pharmaceutical Sciences, The University of Tokyo, Tokyo 113-0033, Japan*

Ryosuke Kojima − *Graduate School of Medicine, The University of Tokyo, Tokyo 113-0033, Japan; PRESTO, Japan Science and Technology Agency, Kawaguchi, Saitama 332-0012, Japan*

Toshitada Yoshihara − *Graduate School of Science and Technology, Gunma University, Kiryu-shi, Gunma 376-8515, Japan;* orcid.org/0000-0002-7960-0740

Seiji Tobita − *Graduate School of Science and Technology, Gunma University, Kiryu-shi, Gunma 376-8515, Japan;* orcid.org/0000-0001-8024-7318

Complete contact information is available at: https://pubs.acs.org/10.1021/jacs.0c00451

Notes

The authors declare no competing financial interest.

ACKNOWLEDGMENTS

This research was supported in part by AMED under grant number JP19gm0710008 (to Y.U.), by JST/PRESTO grant JPMJPR14F8 (to M.K.), by MEXT/JSPS KAKENHI grants JP16H02606, JP26111012, and JP19H05632 (to Y.U.) and JP15H05951 "Resonance Bio", JP19H02826, and JP19K22242 (to M.K.), by JSPS Core-to-Core Program (grant number JPJSCCA20170007), A. Advanced Research Networks, by Japan Foundation for Applied Enzymology (to M.K.), and The Naito Foundation (to M.K.), as well as a stipend from the Graduate Program for Leaders in Life Innovation (GPLLI) and a JSPS stipend (to A.M.). The authors thank S. Manley for sharing the plasmid encoding mitochondria-localizable SNAP-tag and *C. crescentus* bacterial strain (EG603) and for advice on bacterial imaging.

REFERENCES

(1) Nienhaus, K.; Nienhaus, G. U. Where Do We Stand with Super-Resolution Optical Microscopy? *J. Mol. Biol.* **2016**, *428*, 308−322.

(2) Sauer, M.; Heilemann, M. Single-Molecule Localization Microscopy in Eukaryotes. *Chem. Rev.* **2017**, *117*, 7478−7509.

(3) Wu, Y.; Shroff, H. Faster, sharper, and deeper: structured illumination microscopy for biological imaging. *Nat. Methods* **2018**, *15*, 1011−1019.

(4) Blom, H.; Widengren, J. Stimulated Emission Depletion Microscopy. *Chem. Rev.* **2017**, *117*, 7377−7427.

(5) Schermelleh, L.; Ferrand, A.; Huser, T.; Eggeling, C.; Sauer, M.; Biehlmaier, O.; Drummen, G. P. C. Super-resolution microscopy demystified. *Nat. Cell Biol.* **2019**, *21*, 72−84.

(6) Allen, J. R.; Ross, S. T.; Davidson, M. W. Single molecule localization microscopy for superresolution. *J. Opt.* **2013**, *15*, 094001.

(7) Heilemann, M.; van de Linde, S.; Schuttpelz, M.; Kasper, R.; Seefeldt, B.; Mukherjee, A.; Tinnefeld, P.; Sauer, M. Subdiffraction-resolution fluorescence imaging with conventional fluorescent probes. *Angew. Chem., Int. Ed.* **2008**, *47*, 6172−6176.

(8) Folling, J.; Bossi, M.; Bock, H.; Medda, R.; Wurm, C. A.; Hein, B.; Jakobs, S.; Eggeling, C.; Hell, S. W. Fluorescence nanoscopy by ground-state depletion and single-molecule return. *Nat. Methods* **2008**, *5*, 943−945.

(9) Li, H.; Vaughan, J. C. Switchable Fluorophores for Single-Molecule Localization Microscopy. *Chem. Rev.* **2018**, *118*, 9412−9454.
(10) Uno, S.; Kamiya, M.; Morozumi, A.; Urano, Y. A green-light-emitting, spontaneously blinking fluorophore based on intramolecular spirocyclization for dual-colour super-resolution imaging. *Chem. Commun.* **2018**, *54*, 102−105.
(11) Uno, S.; Tiwari, D. K.; Kamiya, M.; Arai, Y.; Nagai, T.; Urano, Y. A guide to use photocontrollable fluorescent proteins and synthetic smart fluorophores for nanoscopy. *Microscopy* **2015**, *64*, 263−277.
(12) Uno, S.; Kamiya, M.; Yoshihara, T.; Sugawara, K.; Okabe, K.; Tarhan, M. C.; Fujita, H.; Funatsu, T.; Okada, Y.; Tobita, S.; Urano, Y. A spontaneously blinking fluorophore based on intramolecular spirocyclization for live-cell super-resolution imaging. *Nat. Chem.* **2014**, *6*, 681−689.
(13) Umezawa, K.; Yoshida, M.; Kamiya, M.; Yamasoba, T.; Urano, Y. Rational design of reversible fluorescent probes for live-cell imaging and quantification of fast glutathione dynamics. *Nat. Chem.* **2017**, *9*, 279−286.
(14) Meister, A.; Anderson, M. E. Glutathione. *Annu. Rev. Biochem.* **1983**, *52*, 711−760.
(15) Smith, C. V.; Jones, D. P.; Guenthner, T. M.; Lash, L. H.; Lauterburg, B. H. Compartmentation of glutathione: implications for the study of toxicity and disease. *Toxicol. Appl. Pharmacol.* **1996**, *140*, 1−12.
(16) Holden, S. J.; Uphoff, S.; Kapanidis, A. N. DAOSTORM: an algorithm for high-density super-resolution microscopy. *Nat. Methods* **2011**, *8*, 279−280.
(17) Babcock, H.; Sigal, Y.; Zhuang, X. A high-density 3D localization algorithm for stochastic optical reconstruction microscopy. *Opt. Nanoscopy* **2012**, *1*, 6.
(18) Huang, F.; Schwartz, S. L.; Byars, J. M.; Lidke, K. A. Simultaneous multiple-emitter fitting for single molecule super-resolution imaging. *Biomed. Opt. Express* **2011**, *2*, 1377−1393.
(19) Min, J.; Vonesch, C.; Kirshner, H.; Carlini, L.; Olivier, N.; Holden, S.; Manley, S.; Ye, J. C.; Unser, M. FALCON: fast and unbiased reconstruction of high-density super-resolution microscopy data. *Sci. Rep.* **2015**, *4*, 4577.
(20) Takeshima, T.; Takahashi, T.; Yamashita, J.; Okada, Y.; Watanabe, S. A multi-emitter fitting algorithm for potential live cell super-resolution imaging over a wide range of molecular densities. *J. Microsc.* **2018**, *271*, 266−281.
(21) Sage, D.; Kirshner, H.; Pengo, T.; Stuurman, N.; Min, J.; Manley, S.; Unser, M. Quantitative evaluation of software packages for single-molecule localization microscopy. *Nat. Methods* **2015**, *12*, 717−724.
(22) Sakabe, M.; Asanuma, D.; Kamiya, M.; Iwatate, R. J.; Hanaoka, K.; Terai, T.; Nagano, T.; Urano, Y. Rational design of highly sensitive fluorescence probes for protease and glycosidase based on precisely controlled spirocyclization. *J. Am. Chem. Soc.* **2013**, *135*, 409−414.
(23) Urano, Y.; Kamiya, M.; Kanda, K.; Ueno, T.; Hirose, K.; Nagano, T. Evolution of fluorescein as a platform for finely tunable fluorescence probes. *J. Am. Chem. Soc.* **2005**, *127*, 4888−4894.
(24) Thompson, R. E.; Larson, D. R.; Webb, W. W. Precise nanometer localization analysis for individual fluorescent probes. *Biophys. J.* **2002**, *82*, 2775−2783.
(25) Yildiz, A.; Forkey, J. N.; McKinney, S. A.; Ha, T.; Goldman, Y. E.; Selvin, P. R. Myosin V walks hand-over-hand: single fluorophore imaging with 1.5-nm localization. *Science* **2003**, *300*, 2061−2065.
(26) Huang, F.; Hartwich, T. M. P.; Rivera-Molina, F. E.; Lin, Y.; Duim, W. C.; Long, J. J.; Uchil, P. D.; Myers, J. R.; Baird, M. A.; Mothes, W.; Davidson, M. W.; Toomre, D.; Bewersdorf, J. Video-rate nanoscopy using sCMOS camera-specific single-molecule localization algorithms. *Nat. Methods* **2013**, *10*, 653−658.
(27) Los, G. V.; Encell, L. P.; McDougall, M. G.; Hartzell, D. D.; Karassina, N.; Zimprich, C.; Wood, M. G.; Learish, R.; Ohana, R. F.; Urh, M.; Simpson, D.; Mendez, J.; Zimmerman, K.; Otto, P.; Vidugiris, G.; Zhu, J.; Darzins, A.; Klaubert, D. H.; Bulleit, R. F.; Wood, K. V. HaloTag: a novel protein labeling technology for cell imaging and protein analysis. *ACS Chem. Biol.* **2008**, *3*, 373−382.
(28) Jones, S. A.; Shim, S.-H.; He, J.; Zhuang, X. Fast, three-dimensional super-resolution imaging of live cells. *Nat. Methods* **2011**, *8*, 499−505.
(29) Dempsey, G. T.; Vaughan, J. C.; Chen, K. H.; Bates, M.; Zhuang, X. Evaluation of fluorophores for optimal performance in localization-based super-resolution imaging. *Nat. Methods* **2011**, *8*, 1027−1036.
(30) van de Linde, S.; Loschberger, A.; Klein, T.; Heidbreder, M.; Wolter, S.; Heilemann, M.; Sauer, M. Direct stochastic optical reconstruction microscopy with standard fluorescent probes. *Nat. Protoc.* **2011**, *6*, 991−1009.
(31) Klein, T.; Loschberger, A.; Proppert, S.; Wolter, S.; van de Linde, S.; Sauer, M. Live-cell dSTORM with SNAP-tag fusion proteins. *Nat. Methods* **2011**, *8*, 7−9.
(32) Chung, T. K.; Funk, M. A.; Baker, D. H. L-2-Oxothiazolidine-4-Carboxylate as a Cysteine Precursor: Efficacy for Growth and Hepatic Glutathione Synthesis in Chicks and Rats. *J. Nutr.* **1990**, *120*, 158−165.
(33) Huang, Y.; Lu, Z.-Y.; Brown, K. S.; Whitehead, A. S.; Blair, I. A. Quantification of intracellular homocysteine by stable isotope dilution liquid chromatography/tandem mass spectrometry. *Biomed. Chromatogr.* **2007**, *21*, 107−112.
(34) Kořínek, M.; Šístek, V.; Mládková, J.; Mikeš, P.; Jiráček, J.; Selicharová, I. Quantification of homocysteine-related metabolites and the role of betaine−homocysteine S-methyltransferase in HepG2 cells. *Biomed. Chromatogr.* **2013**, *27*, 111−121.
(35) Furne, J.; Saeed, A.; Levitt, M. D. Whole tissue hydrogen sulfide concentrations are orders of magnitude lower than presently accepted values. *Am. J. Physiol. Regul. Integr. Comp. Physiol.* **2008**, *295*, R1479−R1485.
(36) Steele, D. S.; Smith, G. L.; Miller, D. J. The effects of taurine on Ca^{2+} uptake by the sarcoplasmic reticulum and Ca^{2+} sensitivity of chemically skinned rat heart. *J. Physiol.* **1990**, *422*, 499−511.
(37) Ono, K.; Akaike, T.; Sawa, T.; Kumagai, Y.; Wink, D. A.; Tantillo, D. J.; Hobbs, A. J.; Nagy, P.; Xian, M.; Lin, J.; Fukuto, J. M. Redox chemistry and chemical biology of H_2S, hydropersulfides, and derived species: Implications of their possible biological activity and utility. *Free Radical Biol. Med.* **2014**, *77*, 82−94.
(38) Keppler, A.; Gendreizig, S.; Gronemeyer, T.; Pick, H.; Vogel, H.; Johnsson, K. A general method for the covalent labeling of fusion proteins with small molecules in vivo. *Nat. Biotechnol.* **2003**, *21*, 86−89.
(39) Keppler, A.; Kindermann, M.; Gendreizig, S.; Pick, H.; Vogel, H.; Johnsson, K. Labeling of fusion proteins of O^6-alkylguanine-DNA alkyltransferase with small molecules in vivo and in vitro. *Methods* **2004**, *32*, 437−444.
(40) Srikun, D.; Albers, A. E.; Nam, C. I.; Iavarone, A. T.; Chang, C. J. Organelle-targetable fluorescent probes for imaging hydrogen peroxide in living cells via SNAP-Tag protein labeling. *J. Am. Chem. Soc.* **2010**, *132*, 4455−4465.
(41) Shim, S. H.; Xia, C.; Zhong, G.; Babcock, H. P.; Vaughan, J. C.; Huang, B.; Wang, X.; Xu, C.; Bi, G. Q.; Zhuang, X. Super-resolution fluorescence imaging of organelles in live cells with photoswitchable membrane probes. *Proc. Natl. Acad. Sci. U. S. A.* **2012**, *109*, 13978−13983.
(42) Carlini, L.; Manley, S. Live Intracellular Super-Resolution Imaging Using Site-Specific Stains. *ACS Chem. Biol.* **2013**, *8*, 2643−2648.
(43) Wombacher, R.; Heidbreder, M.; van de Linde, S.; Sheetz, M. P.; Heilemann, M.; Cornish, V. W.; Sauer, M. Live-cell super-resolution imaging with trimethoprim conjugates. *Nat. Methods* **2010**, *7*, 717−719.
(44) Endesfelder, U.; van de Linde, S.; Wolter, S.; Sauer, M.; Heilemann, M. Subdiffraction-Resolution Fluorescence Microscopy of Myosin-Actin Motility. *ChemPhysChem* **2010**, *11*, 836−840.
(45) Lee, H. L.; Lord, S. J.; Iwanaga, S.; Zhan, K.; Xie, H.; Williams, J. C.; Wang, H.; Bowman, G. R.; Goley, E. D.; Shapiro, L.; Twieg, R. J.; Rao, J.; Moerner, W. E. Superresolution imaging of targeted proteins in fixed and living cells using photoactivatable organic fluorophores. *J. Am. Chem. Soc.* **2010**, *132*, 15099−15101.
(46) Holden, S. J.; Pengo, T.; Meibom, K. L.; Fernandez Fernandez, C.; Collier, J.; Manley, S. High throughput 3D super-resolution

https://dx.doi.org/10.1021/jacs.0c00451
J. Am. Chem. Soc. 2020, 142, 9625−9633

microscopy reveals Caulobacter crescentus in vivo Z-ring organization. *Proc. Natl. Acad. Sci. U. S. A.* **2014**, *111*, 4566−4571.
(47) Xiao, J.; Goley, E. D. Redefining the roles of the FtsZ-ring in bacterial cytokinesis. *Curr. Opin. Microbiol.* **2016**, *34*, 90−96.
(48) Rowlett, V. W.; Margolin, W. The bacterial divisome: ready for its close-up. *Philos. Trans. R. Soc., B* **2015**, *370*, 20150028.
(49) Jacq, M.; Adam, V.; Bourgeois, D.; Moriscot, C.; Di Guilmi, A.-M.; Vernet, T.; Morlot, C. Remodeling of the Z-ring nanostructure during the Streptococcus pneumoniae cell cycle revealed by photoactivated localization microscopy. *mBio* **2015**, *6*, No. e01108-15.
(50) Owens, R. A.; Hartman, P. E. Export of glutathione by some widely used Salmonella typhimurium and Escherichia coli strains. *J. Bacteriol.* **1986**, *168*, 109−114.
(51) Fahey, R. C.; Brown, W. C.; Adams, W. B.; Worsham, M. B. Occurrence of glutathione in bacteria. *J. Bacteriol.* **1978**, *133*, 1126−1129.
(52) Alkhuder, K.; Meibom, K. L.; Dubail, I.; Dupuis, M.; Charbit, A. Glutathione provides a source of cysteine essential for intracellular multiplication of Francisella tularensis. *PLoS Pathog.* **2009**, *5*, No. e1000284.
(53) Pittman, M. S.; Robinson, H. C.; Poole, R. K. A bacterial glutathione transporter (Escherichia coli CydDC) exports reductant to the periplasm. *J. Biol. Chem.* **2005**, *280*, 32254−32261.
(54) Smirnova, G. V.; Muzyka, N. G.; Glukhovchenko, M. N.; Oktyabrsky, O. N. Effects of menadione and hydrogen peroxide on glutathione status in growing Escherichia coli. *Free Radical Biol. Med.* **2000**, *28*, 1009−1016.
(55) Biteen, J. S.; Goley, E. D.; Shapiro, L.; Moerner, W. E. Three-dimensional super-resolution imaging of the midplane protein FtsZ in live Caulobacter crescentus cells using astigmatism. *ChemPhysChem* **2012**, *13*, 1007−1012.

https://dx.doi.org/10.1021/jacs.0c00451
J. Am. Chem. Soc. 2020, 142, 9625−9633